A realistic vapour phase heat transfer model for the weathering of LNG stored in large tanks

Felipe Huerta, Velisa Vesovic*

Department of Earth Science and Engineering, Imperial College London, London SW7 2AZ, United Kingdom

*corresponding author: Tel: +44 20 7594 7352, E-mail: v.vesovic@imperial.ac.uk

Abstract

A new non-equilibrium model relevant to LNG weathering in large storage tanks under constant pressure has been developed. It treats the heat influx from the surroundings into the vapour and liquid phases separately and allows for heat transfer between the two phases. The main heat transfer mechanisms in the vapour phase are assumed to be advection, due to upward flow of evaporated LNG, and conduction.

It has been observed that the vapour temperature increases monotonically as a function of the height, in agreement with recent experimental results. In all the simulations performed the vapour to liquid heat transfer was small, also in line with recent experimental findings, and is estimated to contribute less than 0.3% to boil-off gas rates. The results of this work indicate that the heat transfer by the advective upward flow dominates the energy transfer within the vapour, while the natural convection, in the body of the vapour, can be neglected. The initial liquid filling has a pronounced effect on all the relevant variables, leading to a decrease in vapour temperature and boil-off gas temperature and an increase in boil-off rates. A rule of thumb for estimating the boil-off gas temperature in industrial storage tanks is provided.

Keywords: heat transfer; LNG; cryogenic storage; boil-off gas.

1. Introduction

The global energy sector is undergoing unprecedented change as it transitions from its reliance on fossil fuels to renewables, in the environment of increasing world-wide energy consumption, led by the development of non-OECD countries [1]. In the circumstances, maintaining standards of living, ensuring the energy supply and mitigating the adverse effects of climate change will not be straightforward, especially as some forecasts indicate that a complete transition will take around a century [2]. In this context, natural gas is going to play an important role in the energy mix, because of its competitive cost and lower emissions when compared to other fossil fuels [3]. Unsurprisingly, it is expected that the use of natural gas will rapidly increase, undergoing the biggest increase among fossil fuels [4]. For instance, natural gas demand increased 3% in 2017 alone [5] and its supply is expected to increase by 45% from 2016 to 2040 [3]. Natural gas (NG) is predominantly a hydrocarbon mixture consisting mainly of methane and, in general, lower amounts of other *n*-alkanes and small inorganic molecules. It can be distributed to users directly from the source through pressurized pipelines or it can undergo a liquefaction process and then be distributed as liquefied natural gas (LNG), by marine transportation, to large storage facilities. An increasing number of users are opting for LNG [4] compelled by concerns around the security of supply, as well as the location of major natural gas fields. Hence, LNG has recently undergone a renaissance, not only becoming the preferred way to transport natural gas, but also finding a use as marine and heavy-vehicle fuel [6-9]. In some instances it has been shown that LNG is not only environmentally, but also economically superior to traditional marine fuel and even marine gas oil [10]. Furthermore, the regasification of LNG, that results in large amounts of energy being generated, has led to the development of new technologies and processes to exploit available cold energy [11-15]. Nevertheless there remain some concerns about the environmental impact of such a large increase in LNG trading [16].

LNG is industrially stored in highly insulated tanks at cryogenic temperatures below -160°C, which corresponds to the LNG boiling point at the operating pressure. Although the tanks are highly insulated, they are subject to heat ingress from the surroundings because of the large temperature gradients between LNG and the environment. The heat ingress leads to preferential evaporation of LNG with the most volatile components, methane and nitrogen, predominantly ending in the vapour phase. In large storage tanks, the vapour produced is typically removed to keep the tank pressure constant and is denominated as boil-off gas (BOG). The heat ingress and BOG removal produce weathering of the remaining LNG, as the concentration of the heavier components increases over time. This has major industrial implications, as it can induce safety hazards such as rollover and it limits the NG marketability, as prolonged weathering can make the produced NG out of regulatory spec. In normal industrial operations accurate quantitative knowledge of the weathering process is essential in the allocation of LNG cargoes to particular storage tanks, ensuring the grid suitability of the delivered natural gas in terms of its heating value and anticipating the consequences of loading a new batch of LNG.

Most academic studies on LNG weathering have been focused in modelling weathering in large tanks during long storage periods typical of marine transportation and peak-shaving facilities. Two different modelling approaches can be identified: (i) based on the boil-off ratio (BOR) and (ii) based on heat ingress. The BOR based models predict weathering by using the BOR as a model input, that is obtained from experimental data for specific storage tanks at typical operating conditions [17, 18]. Although BOR based models are frequently used in the industry because of their simplicity, they are not best suited for LNG with high nitrogen content and for scenario testing for LNG tanks for which BOR data might not be available. In contrast, the models based on heat ingress have firmer theoretical foundations and are more generic, as they calculate the BOR and other industry relevant parameters, by means of a heat transfer

model, making use of mass and energy balances and taking into account tank insulation properties. They have been used to model not only large scale storage tanks, but also medium and small sized tanks containing different cryogens.

The first weathering models based on heat ingress were developed in the 1960s, under steady-state assumption, to calculate the wall temperature profiles [19] and to estimate the maximum BOR [20]. Almost three decades later, the interest in LNG storage modelling was revived by the development of the Shah and Aarts model [21], which constituted the first transient model of weathering. The Shah and Arts model was subsequently included as a sub-model in several works which aimed to improve the thermodynamic model [22-25]. In parallel, Chen et al. developed a model of pure methane evaporation on closed storage tanks to predict the pressure and temperature evolution [26] and Adom et al. developed a model to understand the effect of the operating pressure on BOG rates [27]. Recently, Pellegrini and co-workers [28] developed a weathering model which removed the constant thermophysical properties assumption, but simplified the phase equilibrium calculations in order to linearize it. Thereafter, Migliore and collaborators [29] developed a weathering model based on rigorous heat transfer and phase equilibria sub-models that no longer required the constant heat ingress assumption. All the models developed up to this point assumed thermal equilibrium between LNG and its vapour phase.

More recent weathering models have removed the assumption of thermal equilibrium between liquid and vapour phases on the basis of industrial evidence of vapour superheating. Vapour superheating has also been reported in closed, self-pressurizing small and medium storage tanks for a number of different cryogens [30-33]. The non-equilibrium weathering models treat the heat ingress into the vapour and liquid sections of the storage tank separately, which results in the vapour acting as an additional heat source, as a consequence of it being at a higher temperature. Effendy et al. [34] optimized the operation of an LNG storage tank, as a

unit in a regasification terminal, treating the vapour as being superheated by pure convection. Migliore et al. [35] developed a non-equilibrium weathering model for an LNG storage tank considering two limiting scenarios for the heat transfer within vapour, namely pure convection and pure conduction. They concluded that conduction was the predominant heat transfer mechanism, as the full convection model predicted negligible superheating, while the pure conduction model predicted an average increase in vapour temperature of 8K after one year of weathering, for a tank filled at 97% of its volume. This is in line with recently reported vapour superheating observed experimentally for LN_2 evaporation at constant pressure [33] and scant industrial evidence based on LNG weathering in full scale storage tanks [36]. Hence, both theoretical and experimental studies show a vapour superheating and suggest the predominance of conduction as the heat transfer mechanism.

In this work, we take our previous model of Migliore et al. [35] as the starting point and develop an improved and a more realistic model of the vapour phase in a large storage tank. We see the development of the present model complementing the development of the CFD models [37-42], that are by their nature more complex, computationally more expensive and less yielding to providing the necessary physical insight on the interplay between different mechanisms. Hence, the aim of this work is to produce a model that is easier to interpret and use for routine industrial applications by simplifying the hydrodynamics in both liquid and vapour phases, while retaining the dominant weathering mechanisms.

In section 2 we describe the developed model with special emphasis on the modelling of heat transfer in the vapour phase. In section 3 the results and discussion of the weathering process for different scenarios are presented including analysis of vapour temperature profiles, interfacial heat fluxes and BOG rates. A summary and conclusions of the results are given in Section 4.

2. Model development

As already eluded to in the Introduction, the developed model takes our previous model [29, 35] as the starting point. Thus, the LNG tank undergoing weathering has been modelled as a cylindrical tank with the same geometry and insulation properties, as described previously [29, 35]. The operating pressure was taken as constant and slightly above the atmospheric pressure (P=0.1163 MPa), in order to mimic the operation of a large industrial storage tank. The tank is heated from the bottom by an electrical element at a constant rate $\dot{Q}_{\mathrm{slab}}$ to prevent ground freezing, and the tank roof was assumed to be thermally insulated. As the LNG temperature is around -160°C, heat ingresses from the surroundings through the walls into the liquid $(\dot{Q}_{\mathrm{L}})$ and vapour $(\dot{Q}_{\mathrm{V}})$ phases. The model allows for the vapour phase to become superheated and for the exchange of heat to take place through the vapour-liquid interface, at a rate of $\dot{Q}_{\mathrm{VL}}$. The liquid has been assumed to be at its boiling temperature within the whole domain, as at constant pressure the thermal stratification in the liquid is below 1 K [33, 36, 38, 39].

The heat entering the liquid evaporates the LNG at a rate of $\dot{B}_{\mathrm{L}}$, leading to weathering, as the methane and nitrogen preferential evaporate. The change in the liquid composition, as the remaining LNG becomes richer in the heavier components, results in the increase of the LNG boiling temperature. The evaporated LNG ascends through the vapour subsystem, where as a result of heat ingress from outside, it gets heated and consequently becomes less dense. A small fraction of the evaporated LNG accumulates in the vapour space, while, in order to keep the pressure constant, the remainder leaves the system, from the top of the tank, at a rate $\dot{B}$, that measures the boil-off-gas (BOG) removal. A schematic of the physical model of the LNG tank is depicted in Fig. 1.

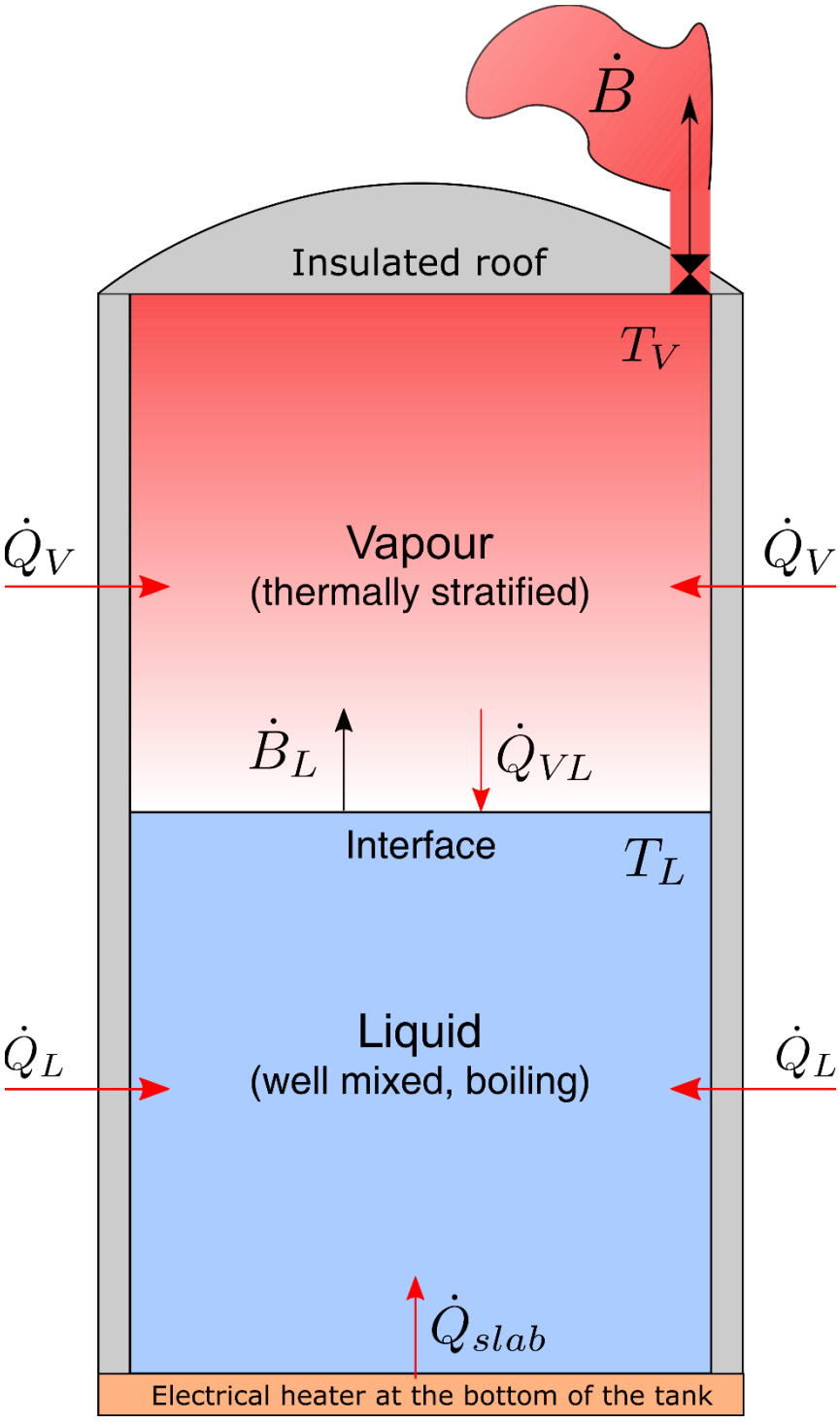

Figure 1: Schematic of the modelled LNG storage tank subject to weathering where the vapour and the liquid subsystems were assumed separated by a smooth, horizontal surface. The red and black arrows represent heat and mass flows, respectively.

The full weathering model is a combination of three sub-models: a mass and energy balance model, a thermodynamic model and a heat transfer model. In the next three subsections, the first two sub-models are described briefly, as more detail can be found in our previous works [29, 35], while the vapour phase heat transfer model, the main novelty of this work, is described in detail.

2.1 Mass and energy balance model

The LNG and its vapour have been assumed to be divided by a smooth vapour-liquid interface and each phase is considered a subsystem. The evaporation rate $\dot{B}_{\mathrm{L}}$ has been obtained by the mass balance on the liquid subsystem as,

$$-\dot{B}_{\mathrm{L}} = \frac{d}{dt}(\rho_{\mathrm{L}} V_{\mathrm{L}}) \,. \tag{1}$$

In a similar way, the BOG removal rate, $\dot{B}$, has been defined as the net mass outflow from the whole tank,

$$-\dot{B} = \frac{d}{dt}(\rho_{\mathrm{L}} V_{\mathrm{L}} + \bar{\rho}_{\mathrm{V}} V_{\mathrm{V}}) = -\dot{B}_{\mathrm{L}} + \frac{d}{dt}(\bar{\rho}_{\mathrm{V}} V_{\mathrm{V}}) \,, \tag{2}$$

where ρ and V are the molar density and molar volume of the mixture, respectively, while the subscripts L and V indicate the liquid and vapour phases, respectively. Performing the energy balance in the liquid phase, provided us with the further expression for the evaporation rate in terms of heat ingress and the mixture thermophysical properties,

$$\dot{Q}_{\mathrm{L}} + \dot{Q}_{\mathrm{slab}} + \dot{Q}_{\mathrm{VL}} - \dot{B}_{\mathrm{L}} h_{\mathrm{V}}(T_{\mathrm{L}}) = \frac{d}{dt}[\rho_{\mathrm{L}} V_{\mathrm{L}} h_{\mathrm{L}}(T_{\mathrm{L}})] \,, \tag{3}$$

where the quantities h and T are the enthalpy and temperature, respectively. One can also re-write Eqs. 1-2 for each species and take advantage of fixed tank volume, see [35] for details, to

end up with an implicit system of $4 + 2 * (n_{\mathrm{comp}} - 1)$ ordinary differential equations (ODE), where n_{comp} is the number of species in the mixture.

2.2 Thermodynamic model

We assumed that the liquid was at physicochemical equilibrium with the vapour interface, and that the vapour composition was spatially homogeneous. The compositions of the vapour and liquid phases are related by $y_i = K_i x_i = (\phi_i^{\mathrm{L}}/\phi_i^{\mathrm{V}}) x_i$, where x_i and y_i are the mole fractions of each species in the liquid and vapour phase, respectively, K_i is the equilibrium constant pertaining to the i^{th} species in the mixture, while the quantities ϕ_i^{L} and ϕ_i^{V} are the fugacity coefficients of liquid and vapour phases, respectively. As previously described [29, 35], the evolution of the composition of the two phases, during the weathering process, was obtained by solving the standard Rachford-Rice equation for the vapour-liquid equilibrium [43]. In order to calculate the fugacity coefficients and all the other required thermophysical properties, except the LNG liquid density, we made use of the Peng-Robinson equation of state (PR-EOS) with the standard Van der Waals mixing rules, that include binary interaction parameters quoted by Danesh [43]. As the cubic equations of state underestimate the liquid density, the liquid LNG density was calculated using the Enhanced Revised Klosek-McKinley correlation [44, 45]. This empirical correlation was specifically developed for LNG and is recommended by the International Group of Liquefied Natural Gas Importers [46] owing to its high accuracy.

As part of this work we compared the accuracy of PR-EOS with the state-of-the-art GERG2008-EOS that was specifically developed for natural gas mixtures [47]. The differences were less than 1% in the BOG rates and in the prediction of the relevant thermophysical properties. Hence, PR-EOS was preferred because of its simplicity and better convergence in flash calculations.

It is worth noting that the thermodynamic model comprises a set of non-linear equations which must be satisfied simultaneously with the ODE system described in the previous section. Hence, the coupled systems of equations constitute a differential algebraic equations (DAE) system.

2.3 Heat transfer model

The heat ingress from the bottom, $\dot{Q}_{\mathrm{slab}}$, has been assumed constant, with a value of 60 kW which is representative of large LNG storage tanks [27]. In line with our previous work, no heat ingress has been assumed to enter through the roof, as in most industrial storage tanks the roof section is separated from the rest of the tank by an insulated suspended deck that acts as a thermal barrier. Inside the tank, the heat ingress through the walls has been delineated between the two phases by the height of the vapour-liquid interface. Conjugate heat transfer has been neglected by assuming no heat accumulation in the tank wall. It is standard practice before filling the industrial LNG storage tanks to precondition the internal wall until the wall temperature reaches a constant value [48]. During preconditioning, the external wall is in contact with the air and hence steady-state heat transfer in the tank wall is established. As the increase in liquid temperature caused by weathering is small, ranging from 0.1 K/year for nitrogen-free LNG to 4 K/year for LNG with 2% by volume of nitrogen [35], neglecting conjugate heat transfer will not affect the heat ingress into the liquid. On the other hand, as the vapour temperature increases appreciably during weathering, neglecting heat accumulation in the tank walls would slightly overestimate the heat ingress into the vapour. It has been assumed that the outer wall is heated by natural convection from the air. The heat then flows, by conduction, across the insulation materials in the radial direction until the inner wall is reached. Finally, the heat is transferred by natural convection to the well mixed liquid, and to a thin buoyant boundary layer within the

vapour phase. As conduction and convection mechanisms are both present, the heat transfer to the liquid and vapour phases were modelled using the overall heat transfer coefficients,

$$\dot{Q}_{\mathrm{L}} = U_{\mathrm{L}} A_{\mathrm{L}} (T_{\mathrm{air}} - T_{\mathrm{L}}) \text{ ,} \quad (4)$$

$$\dot{Q}_{\mathrm{V}} = U_{\mathrm{V}} A_{\mathrm{V}} (T_{\mathrm{air}} - \bar{T}_{\mathrm{V}}) \text{ ,} \quad (5)$$

where U is the overall heat transfer coefficient based on the external contact area, A, between the surrounding air and the tank wall. The liquid and vapour areas, A_{L} and A_{V}, subject to heat ingress from the tank wall, are defined as the area of a cylinder with diameter equal to the external diameter of the tank and a height l equivalent to the height of the liquid and vapour phases, respectively,

Both heat transfer coefficients have been calculated using the procedure described in our previous work [29] based on standard chemical engineering correlations. Note that the calculation of the heat ingress to the vapour across the walls requires a vapour temperature profile, which depends on the vapour phase heat transfer model that will be presented in section *2.3.2*. Hence, the average vapour temperature, $\bar{T}_{\mathrm{V}}$, has been used in the driving force term of Eq. 5.

2.3.1 Vapour to liquid heat transfer model

In the non-equilibrium model, the superheated vapour acts as an additional heat source for the liquid. The vapour to liquid heat transfer rate depends, not only on the temperature difference between the two phases, but also on the heat transfer mechanism in the vapour and at the interface [49, 50]. We have assumed that the heat transfer in the vapour phase is predominantly by conduction, rather than by convection [33, 35, 38]. The slow rate of weathering in large tanks and the negative density gradient in the vapour phase, as a function of

height, support this choice. Furthermore, a number of recent studies on evaporation of different cryogen [31-33] have measured an appreciable, stable vertical temperature gradient within the vapour phase indicating that convective heat transfer is negligible in the vertical direction.

The vapour to liquid heat transfer rate $\dot{Q}_{\mathrm{VL}}$ has been calculated by integrating the heat flux in the vapour phase over the vapour-liquid interface,

$$\dot{Q}_{\mathrm{VL}}(t) = \int_{\mathrm{A_{interphase}}} \boldsymbol{q}|_{z=0} \cdot d\boldsymbol{S} = \int_0^{2\pi} \int_0^{R_{\mathrm{i}}} q_z|_{z=0}\, r dr d\theta \text{ ,} \qquad (6)$$

where $q_{z|z=0}$ is the heat flux across the interface, *r* and θ are the radial and angular coordinates, respectively and z measures the height of the vapour space. The interface has been taken to be a disk of radius equal to the inner radius of the tank R_{i}, orthogonal to the heat flow and smooth. The interface has been assumed smooth because of the relatively low heat fluxes through the liquid. In typical LNG storage tanks, the heat fluxes into the liquid are of the order of 1-10 W/m^2 across the walls and below 20 W/m^2 for slab heating [51]. For example, in the tank modelled in this study the heat flux into the liquid across the walls was 4.4 W/m^2 and the heat flux through the bottom was 13.1 W/m^2. These heat fluxes are well below the nucleate boiling limit and will not greatly perturb the vapour-liquid interface.

Furthermore, we have assumed that the vapour is thermally homogeneous in the radial and azimuthal directions, resulting in an axisymmetric and radially homogeneous temperature profile. The Eq. 6 then reduces to,

$$\dot{Q}_{\mathrm{VL}}(t) = -\pi R_{\mathrm{i}}^2 k_{\mathrm{V}} \left.\frac{\partial T_{\mathrm{V}}}{\partial z}\right|_{z=0}, \qquad (7)$$

where k_{V} is the vapour thermal conductivity evaluated at the interfacial temperature. To calculate the axial temperature gradient in the vapour $(\partial T_{\mathrm{V}}/\partial z)$, a new, realistic 1-D unsteady heat transfer model for the superheated vapour has been developed. The new model improves on the model presented in our previous work [35] in three ways. It removes the assumption of

semi-infinite space, the wall heat ingress is implemented as a volumetric heat source and the heat transported by the ascending evaporative flow is included.

2.3.2 1D heat transfer model of the superheated vapour

A spatial-temporal modelling of the temperature, velocity and concentration fields in the vapour phase would require a full computational fluid dynamics formulation consisting of the Navier-Stokes equations and the species transport equation. In this work, we make the following assumptions to reduce the full continuum model to only the heat transfer equation. First, we consider a spatially homogeneous concentration profile in the vapour instead of solving the species transport equation. Secondly, as most of the BOG is removed as it is generated, to maintain constant pressure, we introduce an advective term characterized by an average vapour velocity in the vertical direction [38] which has been calculated by means of Eq. 2 instead of solving the continuity and momentum equations. Therefore, only the temperature field of the vapour has been modelled by solving the unsteady 1D advection-diffusion equation.

The vapour phase has been modelled as a cylinder with variable height to consider its expansion as the LNG level decreases during weathering. The domain Ω_{1D} is the closed, time-dependant interval $0 < z < l_{\mathrm{V}}(t)$, where $l_{\mathrm{V}}(t)$ is the vapour space height, and it has been calculated at each time-step by solving the coupled mass and energy balances. The vapour is heated by the walls, cooled by the LNG at the interface and insulated at the top simulating a full containment tank. The heat ingress to the vapour phase is carried upwards efficiently by a very thin boundary layer caused by buoyancy driven flow [38, 39, 52]. In the top of the tank, the slightly overheated vapour, which comes from the boundary layer, mixes radially very efficiently. Hence, wall heating has been modelled as a source term $\dot{S}_{\mathrm{wall}}$, under the assumption of well

mixing in the radial direction. Making an usual assumption that the vapour density, heat capacity and thermal conductivity are weak linear functions of temperature [53] one obtains,

$$\frac{\partial T_{\mathrm{V}}}{\partial t} = \bar{\alpha}\frac{\partial^2 T_{\mathrm{V}}}{\partial z^2} - v_z\frac{\partial T_{\mathrm{V}}}{\partial z} + \frac{\bar{\alpha}}{\bar{k}_{\mathrm{V}}}\dot{S}_{\mathrm{wall}}\ , \tag{8}$$

where $\bar{\alpha}$ and $\bar{k}_V$ are the vapour thermal diffusivity and thermal conductivity, respectively, evaluated at the average temperature at each time-step, and v_z is the vapour velocity. The volumetric heat source $\dot{S}_{\mathrm{wall}}$ has been calculated by an energy shell balance as,

$$\dot{S}_{\mathrm{wall}} = \frac{4U_{\mathrm{V}}d_{\mathrm{o}}}{d_{\mathrm{i}}^2}\left(T_{\mathrm{air}} - T_{\mathrm{V}}(z,t)\right)\ . \tag{9}$$

and is a function of both time and height.

Given that the tank pressure is constant, most of the evaporated liquid is removed from the tank, as BOG. As the vapour is being heated, its density will decrease and its velocity will increase. Instead of modelling the vapour velocity by solving the Navier-Stokes equations, we have assumed a spatially homogeneous vapour velocity evaluated at the average vapour density. Furthermore, the velocity profile in the boundary layer has not been modelled explicitly, as the vapour thermal boundary layer thickness for typical LNG large storage tanks has been estimated to be three orders of magnitude lower than the tank radius. Instead, an average vertical vapour velocity has been calculated by dividing the evaporation rate by the interface area and the average vapour density,

$$\bar{v}_z = \frac{4\dot{\mathrm{B}}_{\mathrm{L}}}{\pi d_{\mathrm{i}}^2\bar{\rho}_{\mathrm{V}}}\ . \tag{10}$$

Thus, our final working equation becomes,

$$\frac{\partial T_{\mathrm{V}}}{\partial t} = \bar{\alpha}\frac{\partial^2 T_{\mathrm{V}}}{\partial z^2} - \bar{v}_z\frac{\partial T_{\mathrm{V}}}{\partial z} + \frac{\bar{\alpha}}{\bar{k}_{\mathrm{V}}}\dot{S}_{\mathrm{wall}}\ . \tag{11}$$

Constrained by the following initial and boundary conditions,

$$T_{\mathrm{V}}(t=0,z)=T_{\mathrm{LNG}}(t=0)\,,$$

$$T_{\mathrm{V}}(t,z=0)=T_{\mathrm{LNG}}(t)\,, \tag{12}$$

$$\frac{\partial T_{\mathrm{V}}}{\partial z}(t,z=l_{\mathrm{V}})=\ 0\ ,$$

indicating that: (i) at the beginning of the weathering both vapour and liquid are in thermal equilibrium; (ii) continuity of temperature in the liquid-vapour interface and (iii) the roof is thermally insulated. To summarize, although the PDE proposed in this work, Eq. 11, includes an advective term, $\bar{v}_z \frac{\partial T_{\mathrm{V}}}{\partial z}$, it only has a vertical component and hence, it does not induce convective heat transfer at the interface nor does it lead to natural convection in the whole of the vapour domain. Heat is only transported by conduction and advection in the vertical direction. Thus, the advective term represents the overall upward movement of heat by the ascension of vapour caused by the vertical displacement in the vapour bulk by the denser vapour produced at the interface. For the simulations performed in this work the advective velocities are of the order 8 cm/h.

2.4 Numerical methods

The vapour phase heat transfer PDE, Eq. 11, has been partially discretized using the method of lines [54]. This method consists of transforming the PDE into a system of ordinary differential equations by discretizing explicitly only the spatial dimension. The spatial discretization generates one ODE for each spatial node, and the resulting system has the flexibility to be coupled with other ODE systems. This flexibility is crucial in our model because the three subsystems are coupled and must be solved simultaneously. The diffusion and advection operators in Eq. 11 have been discretized using second order central differences, while the source term has been evaluated at the nodal temperature. The Dirichlet and Neumann

boundary conditions have been implemented using second order central differences with a ghost node, and second order backward differences, respectively. The one-dimensional domain $z = [0, l_V(t)]$ has been discretized into a uniform grid of n_z nodes. The moving boundary has been implemented by transforming the computational grid into a moving mesh, using the coordinate transformation described in Huang and Russell [55]. We chose a grid spacing of Δx = 4cm as a result of a grid sensitivity study for the minimum and maximum liquid fillings. The numerical solution changed by less than 0.03% for BOG rates and by less than 0.01% for average vapour temperatures after halving or doubling the grid spacing.

The mass and energy balances model (Eqs. 1-3) and the equilibrium equation have been augmented with the ODE system produced by the spatial discretization of Eqs. 11-12. Therefore, the weathering model consists of $4 + 2 * (n_{\text{comp}} - 1) + n_z$ ODEs and n_{comp} non-linear equations. It can be classified as a differential algebraic equation (DAE) system of index-1, because the non-linear equations can be converted to ODEs by applying one differentiation step. The flash calculations for phase equilibrium have been implemented using an in-house developed code to solve the Rachford-Rice equation, using the PR-EOS. The transport properties have been evaluated using the REFPROP® 9.0 library [56]. The weathering model has been implemented in MATLAB 2018b®, and the DAE system has been integrated implicitly in time using the ode15i variable-step, variable-order routine [57]. For each equation of the DAE system, the convergence criterium has been set by fixing the absolute and relative tolerances at 10^{-6} and 10^{-3}, respectively. Reducing tolerances by a factor of 10 yields a negligible improvement in the vapour temperatures or BOG rates (<0.01%), at the expense of one order of magnitude longer simulation times. The simulations have been run in a 4-core Intel® Core ™ i7-7700K CPU overclocked at 4300 MHz. The simulation time varied between 2 and 30 seconds depending on the initial composition of the LNG mixtures and the initial liquid filling. These differences arise from the flash subroutine, which converged more slowly for the

methane lean and nitrogen rich LNG mixtures, and for the increased number of nodes required for low initial liquid fillings.

3. Results and Discussion

The developed model has been used to simulate weathering in a typical 165,000 m^3 cylindrical LNG storage tank (d_i = 76.4 m; d_o = 80.0 m;) used by industry. A constant air temperature has been assumed (T_{air} = 298.15 K), which yields the overall heat transfer coefficients of $U_L = U_V$ = 0.038 W m^{-2} K^{-1}. The same tank was employed as in our previous work [29, 35], where the full tank specifications are given, thus allowing for an easy comparison between the two models.

3.1 Temperature profile in the vapour phase

We start by examining the temperature profile in the vapour phase. In order to analyse the heat transfer within the vapour space without complications introduced by weathering of LNG, we have initially modelled LNG as pure methane. For non-nitrogen containing LNG this is an excellent approximation, as studies have shown that the vapour phase primarily consists of methane, until very late in the evaporation cycle [58].

Figure 2a illustrates the transient temperature profiles, as a function of the height of the vapour space, for five specific evaporation periods, namely after 30 hours, 13 weeks, 26 weeks, 39 weeks and 1 year for a tank that was initially filled to 97% of its capacity. We observe very different temperature profiles produced by the current and Migliore et al. model [35]. The former predicts a nearly linear temperature profile as a function of height, while the latter predicts a steep temperature rise in the neighbourhood of the liquid-vapour interface and a nearly constant vapour temperature away from it. We also observe that as evaporation progresses the vapour temperature increases, which is primarily a consequence of the increase in the heat transfer

area. As liquid level decreases due to evaporation, the height of the vapour increases from 1.1 m in the first week to 4.9 m in the last week.

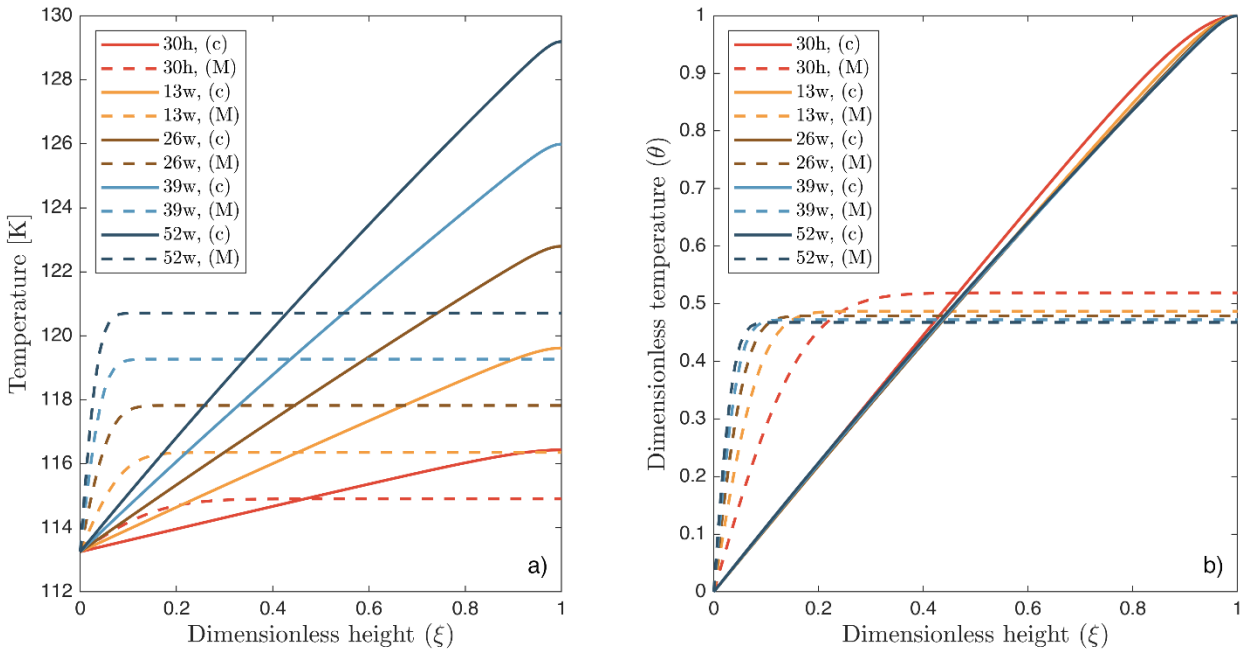

Figure 2: Vapour temperature profiles as a function of height, for transient evaporation of pure methane, in: a) dimensional and b) dimensionless form. (--------) current model (c) and (- - - - -) Migliore et al [35] model (M).

To study the characteristics of the vapour temperature profiles independent of the scale, we have used the following scaling to obtain the dimensionless height (ξ) and dimensionless temperature (θ),

$$\xi = \frac{z}{l_V}\,, \tag{13}$$

$$\theta = \frac{T_V(z) - T_{LNG}}{T_{BOG} - T_{LNG}}\,. \tag{14}$$

Figure 2b illustrates the same transient temperature profiles, but now in dimensionless space. In the new model, the vapour temperature profile undergoes a brief transient period ($t = 30$ hours)

and thereafter becomes quasi-linear for the whole period of evaporation. This profile represents a quasi-steady state similar to the steady state solution of the advection-diffusion equation in the vapour phase, Eq. 11. We also observe, in Fig 2b, that the dimensionless vertical temperature gradient, $\frac{\partial \theta}{\partial \xi}$, is nearly constant for the duration of the evaporation. In contrast, the dimensionless vapour temperature gradient in our previous model [35] is at least one order of magnitude higher in the vicinity of the interface and increases with time, as the average vapour temperature increases rapidly. The temperature profiles in [35] are characteristic of the cooling of a semi-infinite slab. The differences between vapour temperature profiles between the two models are a consequence of the assumptions made in Migliore et al. model [35]. In the new model, we use a finite domain and solve the vapour heat transfer PDE, Eq. (11), coupled with the other sub-models, without assuming homogeneous vapour temperature at every time-step. Hence, a physical transitional period is observed at the onset of steady state, and unrealistically high temperature gradient between the vapour at the interface and the vapour immediately above [35] is no longer observed.

Figure 3 illustrates the variation of the average vapour temperature, $\bar{T}_{\mathrm{V}}$, and the BOG temperature, T_{BOG} , as a function of evaporation time for two models. Although the average vapour temperature calculated by the new model is only slightly higher, the BOG temperature is significantly higher; the difference between two models increases from 3.2 K (2.8%) in the first week to 8.5 K (7%) in the last week. Higher BOG temperature is a direct consequence of the more realistic vapour temperature profile, see Fig 2a. We also observe that in the initial stages of evaporation, both the average and BOG temperatures increase rapidly. We will discuss the reasons for this behaviour in Section 3.3.

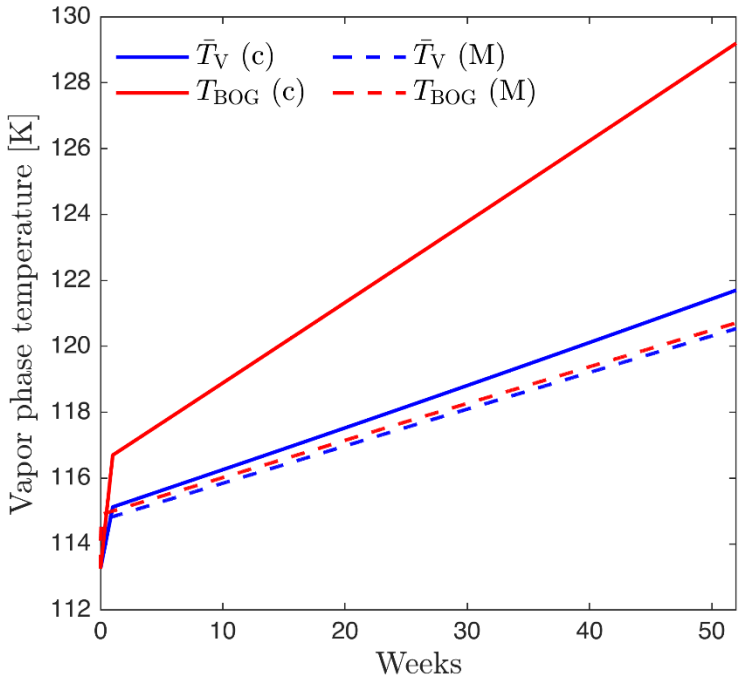

Figure 3: Average vapour temperature, $\bar{T}_V$, and boil-off gas temperature, T_{BOG}, predicted by the current model (c) and Migliore et al. [35] model (M) during the transient evaporation of pure methane.

The initial amount of LNG in the storage tank has a pronounced effect on the evolution of temperature in the vapour space, primarily as a result of the increase in the surface area available for the heat ingress into the vapour. Figure 4 illustrates the temperature profiles for a number of different initial liquid fillings (LF) after 1 and 52 weeks.

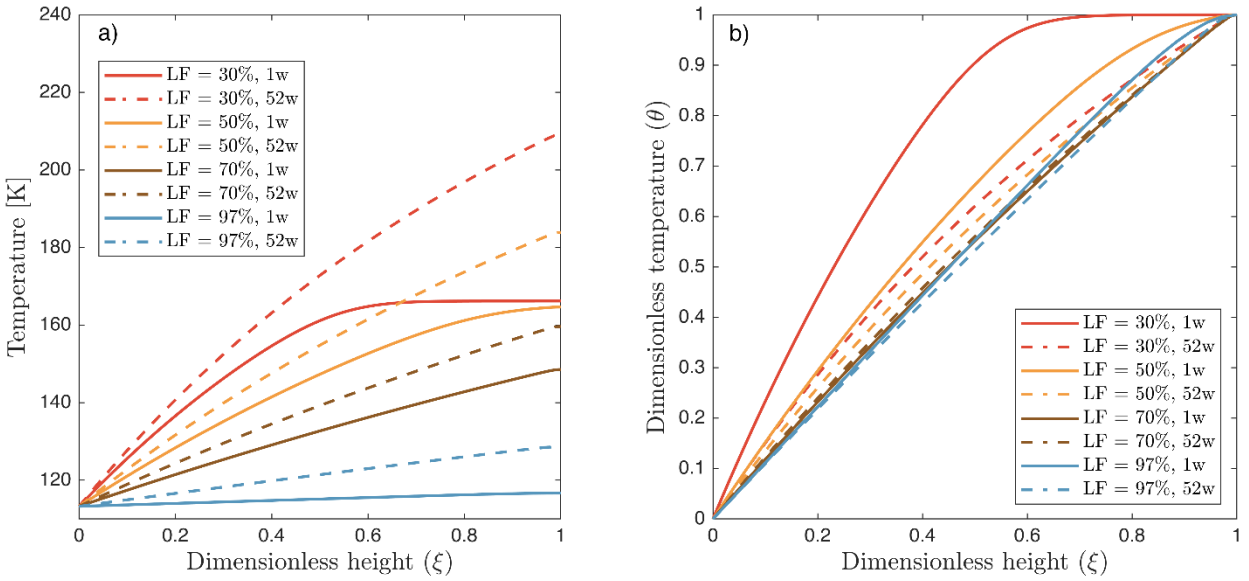

Figure 4: Vapour temperature profiles as a function of height, for transient evaporation of pure methane, in: a) dimensional and b) dimensionless form, for different initial liquid fillings (LF) after 1 and 52 weeks of evaporation.

We observe much higher average and BOG temperatures, the latter reaching 210 K at the end of the 52 week period for 30% initial LNG filling. The higher vapour temperature, that results in the smaller heat flux ingress, and the increase in the vapour height, that decreases the conductive and advective heat transfer, both contribute to slower establishment of the quasi-steady temperature profile.

As far as we are aware there are no experimental data, in open literature, on the vapour temperature profile in industrially sized storage tanks. Nevertheless, over the last few years a number of workers have measured temperature profiles in small tanks of different geometry and for different cryogens [31-33]. The vapour temperature profiles observed for the current model is in good qualitative agreement with recent measurement in vapour temperature in an LNG ship-tank [36] and in the laboratory scale liquid nitrogen tank [33] under isobaric evaporation. In particular, the temperature profiles presented in Fig. 4, align surprisingly well with the profiles

measured by Kang et al. [32] for liquefied nitrogen held in a small 12 l tank. Both the calculated and experimental temperature profiles are linear for high liquid fillings and show slight curvature with increasing temperature gradients near the interface at low liquid fillings. Furthermore, Kang et al. [32] measured a maximum vapour superheating of 31 K for 80% liquid filling, while our model predicts 24 K. This is encouraging agreement, considering the difference in size of the two tanks and the difference in the cryogen used.

The approximately linear vapour temperature profiles observed experimentally indicates that the vapour is cooled vertically, and that temperature is radially homogeneous. Thus, supporting both our assumption on modelling heat transfer as 1-D in z-direction and on modelling vapour flow as purely advective.

3.2 Heat transfer in the vapour phase

Figure 5 illustrates the evolution of the heat ingress into the vapour phase, $\dot{Q}_{\mathrm{V}}$, and vapour to liquid heat transfer rate, $\dot{Q}_{\mathrm{VL}}$, for evaporation of pure methane. We observe that both are lower for the current model, compared with the Migliore et al. [35] model. These results are a direct consequence of the different temperature profiles, illustrated in Fig. 2. As the average vapour temperature in the current model is slightly higher, the driving force $T_{\mathrm{air}} - \bar{T}_{\mathrm{V}}$ in Eq. 5 decreases, producing a slightly lower, of the order of 2%, heat ingress into the vapour $\dot{Q}_{\mathrm{V}}$. For both models, the heat ingress into the vapour increases with time because of an increase in the vapour area A_{V} as the result of evaporation.

We also observe, in Figure 5, that the current model predicts the vapour to liquid heat transfer rate, $\dot{Q}_{\mathrm{VL}}$, to be approximately an order of magnitude smaller than previously reported [35]. Furthermore, in the current model, $\dot{Q}_{\mathrm{VL}}$ slowly increases, from 175 W to 220 W (26%), in one year of weathering, while previously [35] we observed a nearly four-fold increase. These

differences can be ascribed to differences in the predicted temperature gradients at the vapour liquid interphase, see Fig. 2., and an approximate calculational procedure previously adopted [35].

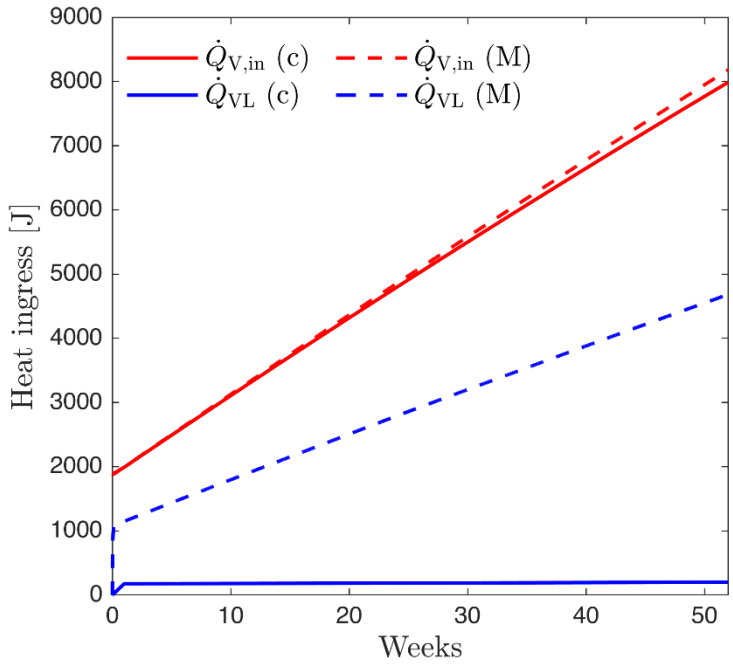

Figure 5: Heat ingress into the vapour, $\dot{Q}_{\mathrm{V,in}}$, and vapour to liquid heat transfer rate, $\dot{Q}_{\mathrm{VL}}$, predicted by the current model (c) and Migliore et al. [35] model (M) during the evaporation of pure methane.

Low $\dot{Q}_{\mathrm{VL}}$ values predicted by the current model align better with recent numerical and experimental studies. Roh and Son [39] developed a CFD model for the transient isobaric evaporation of a pure cryogen and concluded that $\dot{Q}_{\mathrm{VL}}$ contributed less than 0.01% to the total heat ingress into the liquid and was thus negligible. In addition, low $\dot{Q}_{\mathrm{VL}}$ values are consistent with the assumption of dominant heat conduction mechanism at the interface. The suitability of this assumption was experimentally observed by Lin et al. [33], who found that conduction contributed more than 90% of the vapour to liquid heat transfer in LN_2 evaporation in storage

tanks. The nearly constant $\dot{Q}_{\mathrm{VL}}$ during the evaporation suggests the rapid onset of a quasi-steady state, which will be further discussed in 3.3.

We next examine the influence of the initial liquid filling of the storage tank on the heat ingress into the vapour and the vapour to liquid heat transfer rate. As expected, the heat ingress into the vapour $\dot{Q}_{\mathrm{V}}$ increases with decreasing liquid filling (LF), because the vapour area in Eq. 5 increases. However, as illustrated in Fig. 6, the heat flux associated with the heat ingress into the vapour decreases with the initial liquid filling as a direct consequence of increasing average vapour temperatures (see Fig. 4). The initial vapour to liquid heat transfer rate $\dot{Q}_{\mathrm{VL}}$ increases, with decreasing initial liquid filling, from 0.175 kW at 97% LF to 0.275 kW at 30% LF as a direct consequence of larger temperature gradients at the interface. However, the observed 0.1 kW increase in $\dot{Q}_{\mathrm{VL}}$ is negligible compared to the 41.7 kW decrease in $\dot{Q}_{\mathrm{L}}$ because of the decrease in liquid area, A_{L} , between 97% and 30% LF. Overall, the smaller initial liquid filling, results in a smaller heat ingress to the liquid.

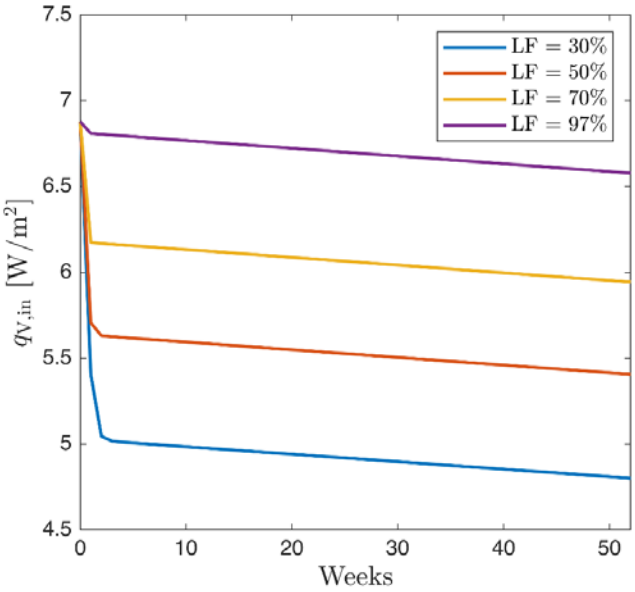

Figure 6: Heat flux into the vapour phase, $q_{\mathrm{V,in}} = \dot{Q}_{\mathrm{V}}/A$, as a function of time for evaporation of pure methane for different initial liquid fillings (LF).

3.3 Analysis of the transient period for the vapour phase heat transfer model and the onset of a quasi-steady state

At early times of evaporation, strong transient dynamics can be observed, as illustrated in Fig. 7. At the beginning of the evaporation, $t = 0$, the vapour temperature is assumed to be equal to the liquid temperature. As the evaporation starts ($t > 0$), we observe, see Fig. 7a and 7b, that the vapour temperature increases rapidly, due to ingress of heat from outside, until a quasi-steady state is achieved. Figure 7c illustrates that a different trend is observed for the heat ingress into the vapour, $\dot{Q}_{\mathrm{V}}$, which initially goes through a minimum before it exhibits a monotonic increase. The initial decrease in $\dot{Q}_{\mathrm{V}}$ can be attributed to a rapid vapour heating, which decreases the difference between the average vapour temperature and the air temperature which drives the heat ingress. The local minimum of $\dot{Q}_{\mathrm{V}}$ is achieved when the decrease in temperature driving force is balanced by the increase in vapour area. Thereafter, $\dot{Q}_{\mathrm{V}}$ increases monotonically as the increase in vapour area dominates the contribution of the increase of average vapour temperature.

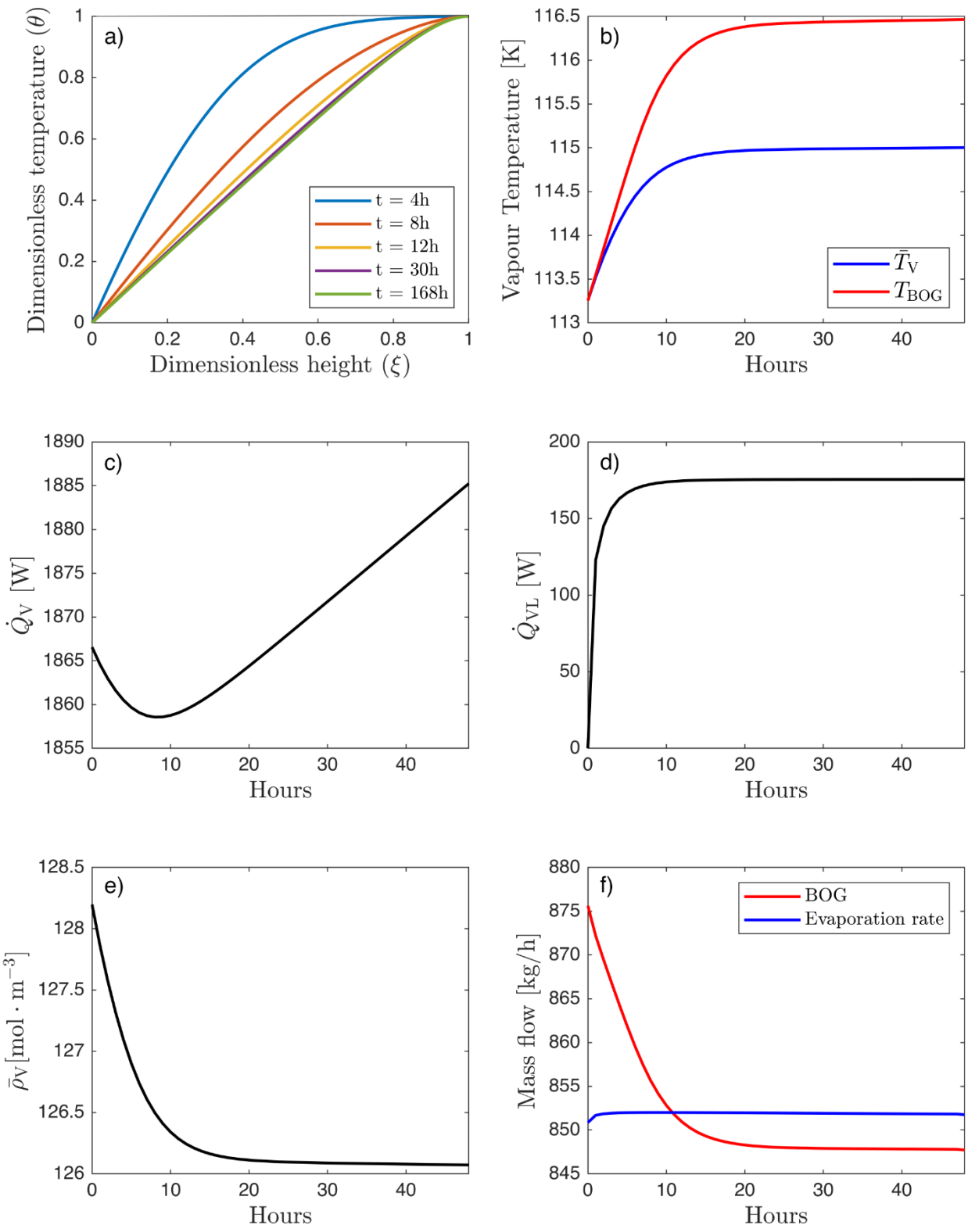

Figure 7: Evolution of process variables during the first 48 hours of the evaporation of pure methane in an LNG storage tank with an initial liquid filling of 97%.

We also observe, in Fig 7d, that the vapour to liquid heat transfer rate, $\dot{Q}_{VL}$, increases rapidly at early times as the temperature gradient at the interface increases. Once the quasi-steady state vapour temperature profile develops, see Figs. 7a and 7b, the vapour to liquid heat transfer reaches a nearly constant value. Figure 7e illustrates that during the transient, the average vapour density rapidly decreases because of the vapour heating. As a consequence of the rapid vapour expansion, the BOG rate at $t = 0$ is maximum and then decreases progressively as the vapour density tends to a quasi-steady state, see Fig 7f. Thereafter, the BOG rate is always lower than the evaporation rate, because a fraction of the evaporated liquid accumulates in the tank to maintain the constant pressure under the conditions of increasing storage tank volume occupied by vapour.

Several recent works [34, 42] attributed the steady-state only to the balance between the heat ingress into the vapour and the vapour to liquid heat transfer rate, on the basis of assuming that natural convection is the predominant heat transfer mechanism in the whole of the vapour phase. The results of the current work indicate that this is not the case. Natural convection in the bulk of the vapour phase is unable to reproduce the vapour superheating observed in industrial set-ups and in experiments, as also demonstrated by Migliore et al. [35]. Furthermore, the presence of natural convection overestimates $\dot{Q}_{\mathrm{VL}}$, [38, 39] and by neglecting the accumulation and BOG removal terms it overestimates the vapour enthalpy. Lin et al. [33] concluded, based on the experimental study of the isobaric evaporation of LN_2 in a semi-spherical tank, that heat conduction contributed more than 90% of the interfacial heat transfer. The vapour to liquid interfacial heat fluxes calculated with our model are lower than 0.1 W/m^2, so we would expect interfacial convective heat transfer of the order of 0.01 W/m^2. In contrast, non-equilibrium weathering models for large tanks which assume natural convection in the vapour,

predict interfacial heat fluxes of 6.9 W/m^2 [42] and 7.6 W/m^2 [34], which most probably overestimate the actual heat flux by at least two orders of magnitude.

The relaxation time, τ, defined as the time to achieve the quasi-steady state for the vapour temperature, was around 30 hours for our specific tank at 97% initial liquid filling. However, applying scaling analysis to Eq. 11, we observe that the relaxation time would depend on a number of parameters. In order to further elucidate the interplay between conduction and advection and establish the dominant heat transport mechanism we ran the model for different axial velocities ($\bar{v}_z$) and initial liquid fillings. For each simulation run, the relaxation time was estimated observing the dimensionless vapour temperature profiles. The variation of relaxation time, τ, as a function of velocity and vapour height are depicted in Figs. 8a and 8b, respectively. We observe that τ is a linear function of l_V and it is inversely proportional to the vapour velocity. Hence, the relaxation time scales as $\tau \sim (l_V/\bar{v}_z)$ which indicates that the vertical advection is the heat transport mechanism which dominates the onset of steady state.

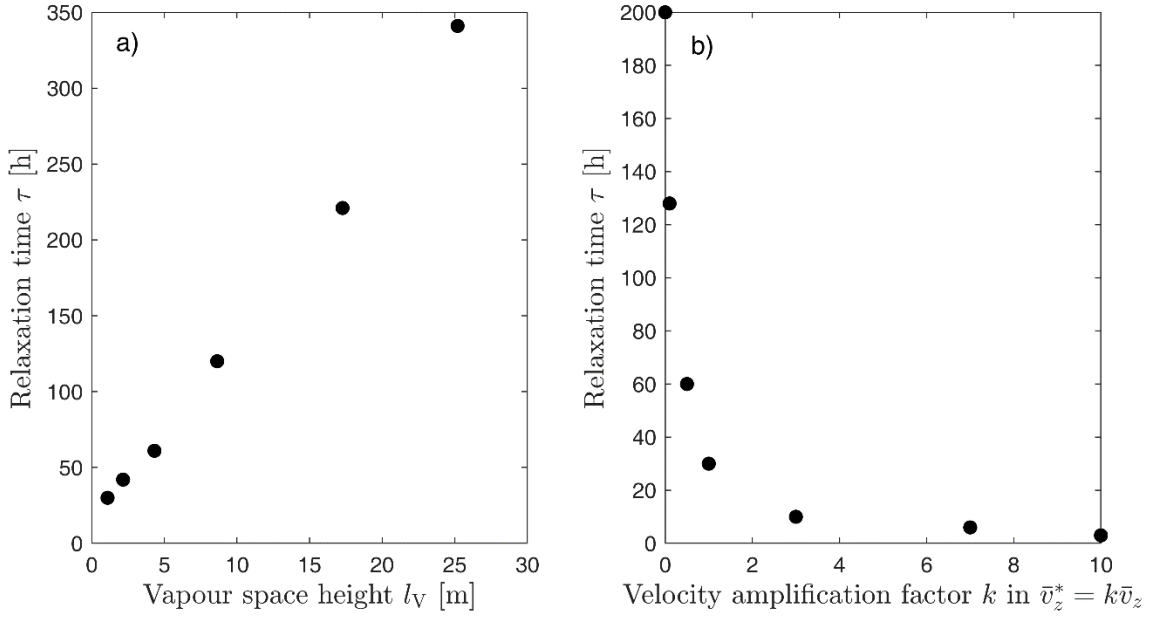

Figure 8: Relaxation time as a function of: a) the vapour height (l_V); and b) the vertical average velocity ($\bar{v}_z^* = k\bar{v}_z$).

We assessed the dominant heat transfer mechanism by calculating the Peclet number, which represents the ratio between advection and conduction, for different liquid fillings using the average vapour velocity $\bar{v}_z$. The Peclet number varied between 10 at the maximum liquid filling to 120 at the minimum liquid filling, indicating the predominance of advection. However, these values of the Peclet number are not high enough to neglect conduction, especially in the case of high liquid fillings. For better insulated tanks where the overall heat transfer coefficients are lower than what was assumed in this work, conduction will become more important as $\bar{v}_z$ will decrease due to lower evaporation rates.

We also examined the effect of the source term, $\dot{S}_{\mathrm{wall}}$, on the relaxation time. For a particular tank, the source term increases with the increasing air temperature and decreases with improvements in tank insulation (see Eq. 9). As a consequence, any increase in the source term will also increase $\bar{v}_z$ because of higher evaporation rates, due to larger heat ingresses into the liquid, and lower average vapour densities, due to higher average vapour temperatures (see Eq. 10). To assess the interplay between the source term and the advective term, the model was run for $U_{\mathrm{V}}{}^{*} \in [0.1U_{\mathrm{V}}, 10U_{\mathrm{V}}]$ and $T_{\mathrm{air}}^{*} \in [T_{\mathrm{air}} - 100, T_{\mathrm{air}} + 100]$ resulting in an overall decrease in the relaxation time with the increase of either the overall heat transfer coefficient or the air temperature. Conversely, decreasing the source term will decrease the advective term, increase the relaxation time and make conduction more significant.

3.4 Boil off gas (BOG) rate for typical LNG mixtures

We now turn our attention to examining the BOG rate for typical LNG mixtures encountered in industry. For this purpose, we used three LNG mixtures studied in our previous work [29, 35], which cover a range of commercially available LNG.

For all three mixtures (Light LNG, Heavy LNG and N_2-rich LNG) we observed very similar temperature profiles and vapour to liquid heat transfer rates as we have observed for evaporation of pure methane, as illustrated in Sections 3.1-3.3. This is not surprising as the vapour phase of both light and heavy LNG is made up primarily of methane during the 52 weeks of weathering. The vapour phase of N_2-rich LNG mixture is initially nitrogen rich, as nitrogen preferentially evaporates [29]. This has a very small effect on temperature profiles and vapour to liquid heat transfer rates as the thermophysical properties of nitrogen vapour are similar to those of methane.

Figure 9 illustrates the BOG rates as a function of weathering for the LNG studied. We observe that the current model predicts lower BOG rates for all LNG mixtures considered in this work compared with the Migliore et al. model [35]. Lower BOG rates are a direct consequence of lower vapour to liquid heat transfer rates, which induce lower evaporation rates. The difference in the BOG rate predictions of the two models increases with the duration of weathering. Taking the Light LNG as an example, the difference in the BOG rate increases from -6.8 kg/h (-0.8%) in the first week to -30.2 kg/h (-3.8%) in the last week, while for Heavy LNG the figures are -0.9% and -3.8%, respectively. For the light and heavy LNG mixtures both models predict a decreasing BOG rate. In contrast, for the N_2-rich LNG mixture both models predict a local maximum. The appearance of the maximum, in the BOG rate, is a consequence of the interplay between the decreasing heat ingress into the liquid and decreasing enthalpy of vaporization, as discussed previously [35]. The current model predicts the maximum in BOG fifteen weeks earlier than the Migliore et al. model [35], because the decrease in the total heat ingress into the liquid during weathering is more rapid, due to $\dot{Q}_{\mathrm{VL}}$ being an order of magnitude lower, as illustrated in Fig. 5.

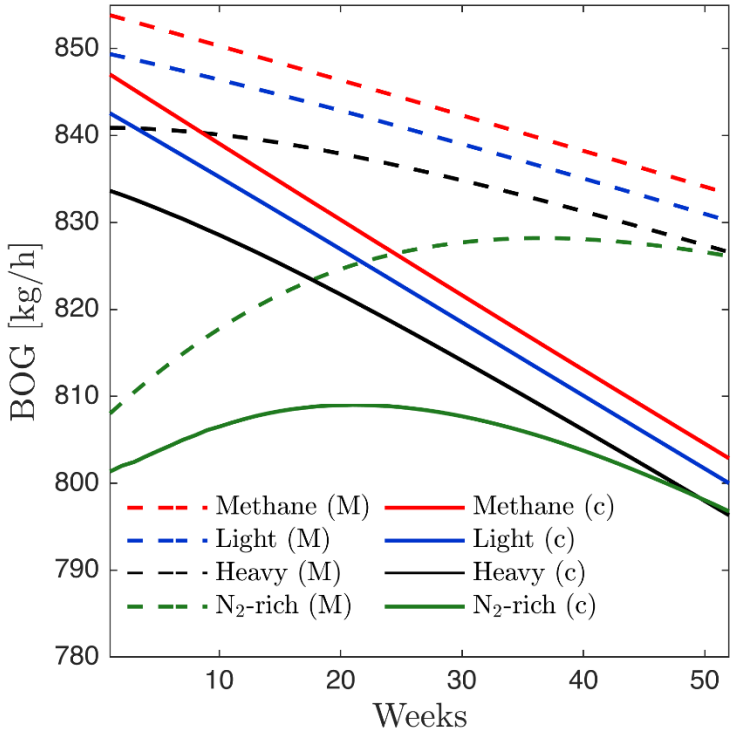

Figure 9: BOG rate as a function of time for three different LNG mixtures: (----------) the current model (c); (- - - - -) Migliore et al. [35] model (M)

3.5 Industrial significance

In this section we explore some of the consequences of the presented results, as far as the design and operations of real LNG storage tanks are concerned.

For the design and operation of LNG storage tanks, determining the BOG temperature is important. We have already established that the relaxation time τ decreases with the increasing of the initial amount of LNG present in the tank. Once the quasi-steady state has been reached, the dimensionless temperature profile is roughly constant, see Fig. 2b, and for high initial liquid fillings it is nearly linear, see Fig. 4b. This would indicate that for high initial liquid fillings, the ratio of temperature difference between T_{BOG} and T_{LNG} and vapour height remains constant

during the subsequent evaporation. Noting that storage times, τ_s, are typically long compared to the transient time, one can propose a rule of thumb to predict the BOG temperature,

$$\frac{\mathrm{T_{BOG}(t)-T_L(t)}}{l_V(t)} \approx \text{constant} \quad \text{for } \tau \ll \tau_s \;\&\; \mathrm{LF} \to 1 \;, \tag{15}$$

For large liquid fillings, the vapour height $l_V(t)$ increases approximately linearly with a constant gradient expressed in terms of the tank characteristics and the mixture thermophysical properties,

$$l_V(t) \approx l_V^0 + \frac{\dot{Q}_L^0 + \dot{Q}_{\mathrm{slab}}}{\pi d_i^2 \rho_L^0 (h_V^0 - h_L^0)} t \;. \tag{22}$$

where t is the time in seconds and the superscript 0 indicates that quantities are evaluated at the initial LNG temperature and vapour height. The rule gives accurate estimates of BOG temperature for LNG storage tanks that are initially filled to 70% or more of their capacity, irrespective of the LNG composition. Taking a worst case scenario, for a storage tank initially filled with 70% of N_2-rich LNG, if one were to use measured BOG temperature and vapour height at the end of first week to predict the BOG temperature in the 12nd and 52nd week, the errors would be just 0.7 K (0.4%) and 1.8 K (1.2%), respectively. For lower initial fillings the deviations are higher, as a result of non-linearity of the quasi–steady temperature profile.

The developed model allows for better characterization of the initial period of evaporation, thus providing a new insight relevant for design and operation of cryogenic control valves, BOG compressors and the gas receiving network. At early times we have observed, as illustrated in Figs. 7b and 7f, a rapid increase in vapour temperature and high BOG rates, compared to variation in both parameters once the quasi steady-state has been reached. The changes will be more pronounced for low initial fillings ($LF \to 0$) corresponding to larger vapour height in a given storage tank. For instance, in a storage tank initially filled with light LNG to 30% of its capacity the BOG temperature will be, after one week of weathering, 100 K higher

than the liquid temperature and the initial BOG rate will be 158% higher than after one week of weathering. The knowledge of rapid variation in both quantities, in the initial transient period, can be used to develop more optimal operations of the gas receiving facilities.

In section 3.4 we discussed that the current model predicts smaller BOG rates than equilibrium and previous non-equilibrium weathering models. This result is of special interest for ballast voyages, where the initial amount LNG is small. For example, using our previous equilibrium and non-equilibrium models [29, 35] would overestimate the BOG rates by 100% and 26%, respectively, for a storage tank filled with initially 30% of light LNG.

4. Conclusions

A new non-equilibrium weathering model has been developed by implementing a realistic heat transfer model in the vapour phase. It represents the weathering of LNG as a transient evaporation of a liquid mixture at constant pressure with continuous BOG removal and as such it is relevant to LNG weathering in large storage tanks. The heat ingress into the vapour from the outside is included as a source term, while the main heat transfer mechanisms in the vapour phase are assumed to be advection and conduction. The former accounting for the upward flow of evaporated LNG. The resulting system of equations has been solved by implementing a moving mesh in the vapour subdomain and using adaptive time-steps for time integration. The former is necessary to correctly represent the downwards displacement of the vapour-liquid interface, while the latter captures the initial transient behaviour.

Following an initial, transient period, the vapour temperature achieves a pseudo-steady state profile, displaying a monotonic increase as a function of the height of the vapour space in agreement with recent experimental results. The transient time strongly depends on the initial filling of the LNG tank, with the nearly full tanks taking least time to reach the steady-state. As the initial liquid filling decreases, so does the amount of heat entering the liquid, leading to a smaller evaporation rate and smaller heat transfer within the vapour. Consequently, it takes longer for a steady-state vapour temperature profile to be established. During the transient period we observed an interesting array of behaviour with steep changes in vapour temperature and density, vapour to liquid heat transfer and in BOG.

In all the simulations performed the vapour to liquid heat transfer was small, in line with recent experimental findings, and has been estimated to contribute less than 0.3% to BOG rates. In general, less than 10% of the heat that enters vapour is transferred to the liquid, and the amount decreases as weathering progresses, indicating that the vapour phase constitutes an effective thermal resistance. The results of this work taken in conjunction with previous

modelling studies and supported by experimental observation indicate that the heat transfer by the advective upward flow dominates the energy exchange in the vapour phase. Although conduction is important and should be an integral part of any model, it alone would overestimate the vapour to liquid heat transfer rates and lead to larger than expected BOG. Furthermore, the results of the present study further support the assumption of negligible natural convection within the vapour phase.

It has been observed that the BOG rate decreases as a function of weathering duration for non-nitrogen containing LNG. The presence of nitrogen leads to a maximum in BOG that is a result of the interplay between the decreasing heat ingress into the liquid and decreasing enthalpy of vaporization. The BOG temperature increases during weathering and has been shown to be a strong function of the initial liquid filling. For storage tanks that are initially more than 70% filled a simple rule-of-thumb formula has been provided to help estimate the BOG temperature. The developed model allows for the optimization of LNG storage tank operations and different scenario planning taking into account the initial liquid filling and nitrogen content.

The developed 1D vapour superheated model is accurate as long as the pressure of the tank is constant and liquid thermal stratification is not significant, as is the case for large storage tanks that rely on BOG to maintain constant pressure. To model closed tanks, the pressure build-up and liquid thermal stratification must be taken into account. In future work, we aim to include a CFD sub-model for the liquid phase to represent the complex coupling between natural convection, pressure build-up and phase change.

Acknowledgments

F. Huerta would like to acknowledge a postgraduate grant from the National Commission for Scientific and Technological Research (CONICYT) of Chile (CONICYT PFCHA/DOCTORADO BECAS CHILE/2017 – 72180177) that supported his work.

Abbreviations:

BOG: Boil-off gas

BOR: Boil-off ratio

CFD: Computational fluid dynamics

DAE: Differential algebraic equation

LF: Liquid filling

LN_2: Liquefied nitrogen

LNG: Liquefied natural gas

NG: Natural gas

ODE: Ordinary differential equation

PDE: Partial differential equation

PR-EOS: Peng Robinson equation of state

References

[1] International energy outlook 2017. Washington, DC 20585: U.S. Energy Information Administration; 2017.
[2] Warner KJ, Jones GA. The climate-independent need for renewable energy in the 21st century. Energies. 2017;10(8).
[3] World energy outlook 2017. France: International Energy Agency; 2017.
[4] BP Energy outlook 2018. London: BP; 2018.
[5] Global energy and CO2 status report. Paris, France: International Energy Agency; 2018.
[6] Lowell D, Wang H, Lutsey N. Assessment of the fuel cycle impact of liquefied natural gas as used in international shipping. The International Council on Clean Transportation; 2013.
[7] Burel F, Taccani R, Zuliani N. Improving sustainability of maritime transport through utilization of Liquefied Natural Gas (LNG) for propulsion. Energy. 2013;57:412-20.
[8] Song HQ, Ou XM, Yuan JH, Yu MX, Wang C. Energy consumption and greenhouse gas emissions of diesel/LNG heavy-duty vehicle fleets in China based on a bottom-up model analysis. Energy. 2017;140:966-78.
[9] Kwak DH, Heo JH, Park SH, Seo SJ, Kim JK. Energy-efficient design and optimization of boil-off gas (BOG) re-liquefaction process for liquefied natural gas (LNG)-fuelled ship. Energy. 2018;148:915-29.
[10] Yoo BY. Economic assessment of liquefied natural gas (LNG) as a marine fuel for CO2 carriers compared to marine gas oil (MGO). Energy. 2017;121:772-80.
[11] He T, Chong ZR, Zheng J, Ju Y, Linga P. LNG cold energy utilization: Prospects and challenges. Energy. 2019;170:557-68.
[12] Ma G, Lu H, Cui G, Huang K. Multi-stage Rankine cycle (MSRC) model for LNG cold-energy power generation system. Energy. 2018;165:673-88.
[13] Pattanayak L, Padhi BN. Thermodynamic analysis of combined cycle power plant using regasification cold energy from LNG terminal. Energy. 2018;164:1-9.
[14] Le S, Lee J-Y, Chen C-L. Waste cold energy recovery from liquefied natural gas (LNG) regasification including pressure and thermal energy. Energy. 2018;152:770-87.
[15] Lee I, Park J, Moon I. Conceptual design and exergy analysis of combined cryogenic energy storage and LNG regasification processes: Cold and power integration. Energy. 2017;140:106-15.
[16] Gilbert AQ, Sovacool BK. US liquefied natural gas (LNG) exports: Boom or bust for the global climate? Energy. 2017;141:1671-80.
[17] Miana M, Del Hoyo R, Rodrigálvarez V. Comparison of evaporation rate and heat flow models for prediction of Liquefied Natural Gas (LNG) ageing during ship transportation. Fuel. 2016;177:87-106.
[18] Miana M, Del Hoyo R, Rodrigálvarez V, Valdés JR, Llorens R. Calculation models for prediction of Liquefied Natural Gas (LNG) ageing during ship transportation. Appl Energy. 2010;87(5):1687-700.
[19] Churchill SW. Heat leakage and wall temperature profiles for above ground low-temperature storage tanks. Chem Eng Prog. 1962;58(11):55-60.
[20] Neill DT, Hashemi HT, Sliepcevich CM. Boil-off rates and wall temperatures in above ground LNG storage tanks. Chem Eng Prog Symp. 87 ed: American Institute of Chemical Engineers.; 1968. p. 111-9.
[21] Shah JM, Aarts JJ. Effect of weathering of LNG in storage tanks. Adv Cryog Eng. Boston: Springer US; 1995. p. 253-60.
[22] Kountz KJ. Weathering of LNG in on-board storage tanks. Chicago: Institute of Gas Technology; 1999. p. 1-15.
[23] Aspelund A, Gjøvåg G, Nekså P, Kolsaker K. LNG—Chain, a calculation tool for natural gas quality in small scale LNG distribution chains. ICEC-21 International Cryogenic Engineering Conference 2007.

[24] Aspelund A, Gundersen T, Myklebust J, Nowak MP, Tomasgard A. An optimization-simulation model for a simple LNG process. Comput Chem Eng. 2010;34(10):1606-17.
[25] Dimopoulos GG, Frangopoulos CA. A dynamic model for liquefied natural gas evaporation during marine transportation. Int J Thermodyn. 2008;11(3):123-31.
[26] Chen QS, Wegrzyn J, Prasad V. Analysis of temperature and pressure changes in liquefied natural gas (LNG) cryogenic tanks. Cryogenics. 2004;44(10):701-9.
[27] Adom E, Sheikh ZI, Xianda J. Modelling of boil off gas in LNG tanks: a case study. IJET. 2010;2(4):292-6.
[28] Pellegrini LA, Moioli S, Brignoli F, Bellini C. LNG technology: the weathering in above-ground storage tanks. Industrial & Engineering Chemistry Research. 2014;53(10):3931-7.
[29] Migliore C, Tubilleja C, Vesovic V. Weathering prediction model for stored liquefied natural gas (LNG). J Nat Gas Sci Eng. 2015;26:570-80.
[30] Arnett RW, Voth RO. A computer program for the calculation of thermal stratification and self-pressurization in a liquid hydrogen tank. National Aeronautics and Space Administration; 1972.
[31] Seo M, Jeong S. Analysis of self-pressurization phenomenon of cryogenic fluid storage tank with thermal diffusion model. Cryogenics. 2010;50(9):549-55.
[32] Kang M, Kim J, You H, Chang D. Experimental investigation of thermal stratification in cryogenic tanks. Exp Therm Fluid Sci. 2018;96:371-82.
[33] Lin Y, Ye C, Yu YY, Bi SW. An approach to estimating the boil-off rate of LNG in type C independent tank for floating storage and regasification unit under different filling ratio. Appl Therm Eng. 2018;135:463-71.
[34] Effendy S, Khan MS, Farooq S, Karimi IA. Dynamic modelling and optimization of an LNG storage tank in a regasification terminal with semi-analytical solutions for N2-free LNG. Comput Chem Eng. 2017;99:40-50.
[35] Migliore C, Salehi A, Vesovic V. A non-equilibrium approach to modelling the weathering of stored Liquefied Natural Gas (LNG). Energy. 2017;124:684-92.
[36] Krikkis RN. A thermodynamic and heat transfer model for LNG ageing during ship transportation. Towards an efficient boil-off gas management. Cryogenics. 2018;92:76-83.
[37] Khelifi-Touhami MS, Benbrik A, Lemonnier D, Blay D. Laminar natural convection flow in a cylindrical cavity application to the storage of LNG. J Pet Sci Eng. 2010;71(3):126-32.
[38] Roh S, Son G. Numerical study of natural convection in a liquefied natural gas tank. J Mech Sci Technol. 2012;26(10):3133-40.
[39] Roh S, Son G, Song G, Bae J. Numerical study of transient natural convection in a pressurized LNG storage tank. Appl Therm Eng. 2013;52(1):209-20.
[40] Maksimov VI, Nagornova TA, Glazyrin VP, Shestakov IA. Analysis of influence of heat insulation on the thermal regime of storage tanks with liquefied natural gas. Thermophysical Basis of Energy Technologies 2015 Tomsk, Russia: EPJ; 2016. p. 01042:1-7.
[41] Choi SW, Lee WI, Kim HS. Numerical analysis of convective flow and thermal stratification in a cryogenic storage tank. Numer Heat Transfer, Part A. 2017;71(4):402-22.
[42] Saleem A, Farooq S, Karimi IA, Banerjee R. A CFD simulation study of boiling mechanism and BOG generation in a full-scale LNG storage tank. Comput Chem Eng. 2018;115:112-20.
[43] Danesh A. PVT and phase behaviour of petroleum reservoir fluids. 1st ed: Elsevier, 1998.
[44] Tietz C, Richter M, Kleinrahm R, Span R. Enhancement of the revised Klosek and McKinley method for density calculations of liquefied natural gas (LNG) over the temperature range from (100 to 135) K at pressures up to 10 MPa. Fuel Process Technol. 2017;165:19-26.
[45] Klosek J, McKinley C. Densities of liquefied natural gas and of low molecular weight hydrocarbons. Conference Densities of liquefied natural gas and of low molecular weight hydrocarbons, Chicago.

[46] LNG custody transfer handbook. 5th ed. Neuilly'sur'Seine, France: The International Group of Liquefied Natural Gas Importers (GIIGNL); 2017.
[47] Kunz O, Wagner W. The GERG-2008 wide-range equation of state for natural gases and other mixtures: an expansion of GERG-2004. J Chem Eng Data. 2012;57(11):3032-91.
[48] LNG Information paper No. 2 the LNG process chain. Neuilly'sur'Seine, France: The International Group of Liquefied Natural Gas Importers (GIIGNL); 2009.
[49] Kassemi M, Kartuzova O, Hylton S. Validation of two-phase CFD models for propellant tank self-pressurization: Crossing fluid types, scales, and gravity levels. Cryogenics. 2018;89:1-15.
[50] Nawaz W, Olewski T, Véchot L. Assessment and validation of evaporation models for cryogenic liquids. Process Saf Env. 2019;121:50-61.
[51] Lisowski E, Czyżycki W. Transport and storage of LNG in container tanks. Journal of KONES Powertrain and Transport. 2011;18(3):193-201.
[52] Gursu S, Sherif SA, Veziroglu TN, Sheffield JW. Analysis and optimization of thermal stratification and self-pressurization effects in liquid-hydrogen storage-systems - Part 2: Model results and conclusions. J Energ Resour-Asme. 1993;115(3):228-31.
[53] Bird RB, Stewart WE, Lightfoot EN. Transport phenomena. 2nd rev. ed. New York: John Wiley & Sons, 2007.
[54] Schiesser WE, Griffiths GW. A compendium of partial differential equation models: method of lines analysis with Matlab. 1st ed. Cambridge ; New York: Cambridge University Press, 2009.
[55] Huang W, Russell RD. Adaptive moving mesh methods: Springer Science & Business Media, 2010.
[56] Lemmon; EW, Huber; ML, McLinden MO. NIST Standard Reference Database 23: Reference Fluid Thermodynamic and Transport Properties-REFPROP, Version 9.1, National Institute of Standards and Technology. 2013.
[57] Shampine LF. Solving 0 = F(t, y(t), y'(t)) in Matlab. J Num Math. 2010;10(4):19.
[58] Conrado C, Vesovic V. The influence of chemical composition on vaporisation of LNG and LPG on unconfined water surfaces. Chem Eng Sci. 2000;55(20):4549-62.